6.7

Paper No. 5

THE EFFECT OF BLADE ELASTICITY ON THE DESIGN
OF A WIND TURBINE

Keiji KAWACHI and Akira AZUMA

Institute of Interdisciplinary Research
Faculty of Engineering, The University of Tokyo
4−6−1, Komaba, Meguro-ku,
Tokyo, 146 Japan

September 8−11, 1987

ARLES, FRANCE

THE EFFECT OF BLADE ELASTICITY
ON THE DESIGN OF A WIND TURBINE

Keiji KAWACHI and Akira AZUMA
Institute of Interdisciplinary Research
Faculty of Engineering, The University of Tokyo
Tokyo, Japan

ABSTRACT

An analytical study has been conducted in order to make clear effects of the blade elasticity on the design of a horizontal axis wind turbine. Coupled flap-lag-torsion equations of motion of an isolated rotor blade have been solved with the aerodynamic force obtained by the Local Circulation Method. The sensitivity of various parameters such as rigidity, pitch angle, position of center of gravity and position of elastic axis of the blade for flutter boundary is presented. In addition, a difference of the flutter boundary between hingeless and seesaw rotors is presented. The procedure taking these parameters into the design consideration is completed. The re-design of an exemplified rotor, which has been actually built and operated, is attempted by following this flow chart. The result indicates that the rigidity and the mass of the blade may be reduced to half values of the original blade.

1. Nomenclatures

a	nondimensional position of elastic axis based on the half chord
b	half chord length
$C(k)$	Theodorsen function
$C_\ell (\alpha)$	lift coefficient
EI_y, EI_z, EI_{yz}	bending rigidities
e_{Ay}, e_{Az}	position of center of surface
e_y	distance between feathering axis and elastic axis
$\bar{e}_y$, $\bar{e}_z$	position of gravity center of blade section
F_y, F_z	external forces given by eq. (A-4) and (A-5)
$F(k)$	real part of Theodorsen function
GJ	torsional rigidity
g	gravity acceleration
h	normal displacement of a blade element, positive downward
$\bar{I}_x$, $\bar{I}_y$, $\bar{I}_z$, $\bar{I}_{yz}$	moments of inertia per unit length
i	inclination angle of tip-path-plane with respect to the general flow

j_A	number of modes of articulated modal series
j_R	number of modes of rigid modal series
k	reduced frequency
k_A	radius of gyration
L_y, L_z	aerodynamic forces along y and z axes respectively
ℓ	lift acting on a blade element $= \ell_1 + \overline{\ell_2} + \Delta\ell_2$
ℓ_1	apparent mass component of the lift ℓ
ℓ_2	circulatory component of the lift ℓ
M_b	blade mass
M_j	generalized mass
M_x	aerodynamic moment about x axis
N_x	external moment given by eq. (A-6)
m	blade mass per unit span or moment acting on a blade element $= m_1 + \overline{m_2} + \Delta m_2$
m_1	apparent mass component of the moment m
m_2	circulatory component of the moment m
Q_j	generalized force
q	amplitude of mode
R	rotor radius
r	radius position of rotor blade
$S(k)$	Sears function
T	spanwise tension
U	stationary inflow velocity $= \sqrt{U_{\overline{T}}^2 + U_{\overline{P}}^2}$
U_T	tangential component of the inflow velocity
$U_{\overline{T}}$	stationary component of U_T
U_P	normal component of the inflow velocity
$U_{\overline{P}}$	stationary component of U_P
u_c, v_c, w_c	displacement of elastic axis
V	wind velocity
v^j	induced velocity generated by the preceding j-th blade
Δv	induced velocity generated by the blade under consideration
x	nondimensional distance $= r/R$
α	angle of attack of a blade element $= \theta - \phi$
α_G	angle of attack caused by the induced velocity $= -(\sum_j v^j + \Delta v)/U$
β_p	preconing angle
θ	feathering angle
μ	advance ratio $= V\cos i/R\Omega$

ρ	air density
ϕ	stationary inflow angle $= \tan^{-1}(-U_{\bar{P}}/U_{\bar{T}})$
ϕ_c	torsional axis
ψ	azimuth angle $= \Omega t$
Ω	rotational speed
ω	frequency of natural vibration
$(\dot{\ })$	time derivative $= (d/dt)$
$(\ )'$	spanwise derivative $= (d/dr)$
$(\bar{\ })$	stationary value or mean value
$(\hat{\ })$	mode of natural vibration
$(\ )^A$	quantity of articulated modal series
$(\ )^R$	quantity of rigid modal series
$\Delta(\ )$	variational value

2. Introduction

It has been paid attention to the classical flutter, coupled vibration of bending and torsional motions, of rotary wings as well as fixed wings in many years. Since the respective blade of rotary wing is operated in a field of large centrifugal force and of strong downwash left by the preceding blades, more sophisticated analysis is required than that of fixed wings.

The linear perturbation method was proposed by Feingold[1] assuming the uniform induced velocity distribution over the rotor disc. The Floquet's theorem[2]-[3] was applied to extend the capability of calculation to the rotor operating in an inclined flow. In order to take the non-uniform induced velocity distribution into the calculation, vortex theory[4]-[5] was proposed to the analyses of the flutter. However, the assumption of the uniform induced velocity distribution sometimes causes inaccurate results, and also vortex theory usually requires much computational time.

Improvement of these theories has been attained by the Local Circulation Method (LCM), in which fully coupled elastic equations of motion of a turbine blade are combined with the calculation of the dynamic airloading acting on the deformed blade.[6] Results of this analytical method were compared with those obtained by vortex theory and with the experimental data.

Fig. 1[7] shows the results of the calculations for a helicopter model blade. This blade was designed to investigate experimentally the bending-torsion flutter in the wind tunnel. It had two hinges with spring stiffness for flapping and torsional motion, and was rigidly constrained for lead-lag motion. It is observed from the figure that the LCM has the capability of achieving a level of accuracy similar to that of lifting surface vortex theory[8] by using a much smaller amount of a computational time.

Fig. 2[6] shows a comparison in flutter boundary between the LCM and the experiment for a wind turbine model blade. This blade was hingeless, and had simulated rigidity and mass distributions along the blade span for a real rotor. It is observed that a good correlation is again obtained between the analysis and the experiment, although the experimental result is limited for one operational case. This is because the model blade was actually destroyed by the flutter.

In the present study, an analytical method of computation is developed in order to make clear the effect of the flutter boundary on the design of horizontal axis wind turbines.

3. Analytical Method

Aerodynamic force and moment are calculated by the LCM concerning unsteady aerodynamic effects as follows:

Tangential and normal components of inflow velocity with respect to a blade element are given respectively by

$$U_T = R\Omega (x+\mu\sin\psi) + (\sum_j v^j + \Delta v) \sin\phi + \dot{v}_c$$

$$U_P = -R\Omega\mu\tan i + (\sum_j v^j + \Delta v) \cos\phi - \dot{w}_c - R\Omega w'_c \mu\cos\psi \tag{1}$$

where

$$\phi = \tan^{-1} (-U_{\overline{P}}/U_{\overline{T}})$$

$$U_{\overline{P}} = -R\Omega\mu\tan i - \dot{w}_c - R\Omega w'_c \mu\cos\psi \tag{2}$$

$$U_{\overline{T}} = R\Omega (x+\mu\sin\psi) + \dot{v}_c .$$

Then the lift and moment of the blade element can be given by

$$\ell = \ell_1 + \bar{\ell}_2 + \Delta\ell_2$$

$$m = m_1 + \bar{m}_2 + \Delta m_2 \tag{3}$$

where $( )_1$ and $( )_2$ show the apparent mass components and circulatory components respectively, and where $\bar{( )}$ and $\Delta( )$ show the stationary component and the variational component, respectively. They are, hence, given by

$$\ell_1 = \rho\pi b^2 (\ddot{h} + U\dot{\alpha} - ab\ddot{\alpha})$$

$$\bar{\ell}_2 = \rho U^2 b \{C_\ell(\bar{\alpha}) + C_\ell (\bar{\alpha}_G) \}$$

$$m_1 = \rho\pi b^3 \{a\ddot{h} - U (\frac{1}{2} - a)\dot{\alpha} - b (\frac{1}{8} + a^2)\ddot{\alpha} \} \tag{4}$$

$$\bar{m}_2 = b (a + \frac{1}{2}) \bar{\ell}_2$$

$$\Delta\ell_2 = \rho U^2 b \{C(k) \ C_\ell(\Delta\alpha) + S(k) \ C_\ell(\Delta\alpha_G)\}$$

$$\Delta m_2 = b \ (a + \frac{1}{2}) \ \Delta\ell_2 \tag{5}$$

$$U = \sqrt{U_T^2 + U_P^2}$$

$$\dot{h} = \{-\ \dot{w}_c - R\Omega w_c' \mu\cos\psi\} \ \cos\phi + \dot{v}_c \sin\phi$$

$$\alpha = \bar{\alpha} + \Delta\alpha = \theta - \phi = \theta - \tan^{-1}(-U_P/U_T) \tag{6}$$

$$\alpha_G = \bar{\alpha}_G + \Delta\alpha_G = -(\sum_j v^j + \Delta v)/U$$

where the induced velocity mainly generated by the trailing vorticies, $\sum_j v^j + \Delta v$, has been regarded as if there is a vertical gust for the blade element. The effect of shed vortices on the lift and moment has been represented by the Theodorsen and Sears functions.[9]

The equations of the blade elasticity are given in Appendix A, for the displacement parpendicular to the rotational plane, w_c, the displacement parallel to the rotational plane, v_c, and the torsional displacement, ϕ_c. For the hingeless blade, these equations are solved simultaneously by the mode expansion method,

$$\{w_c(r,t), v_c(r,t), \phi_c(r,t)\}^T = \sum_{j=1}^{j} \{\hat{w}_j(r), \hat{v}_j(r), \hat{\phi}_j(r)\}^T q_j(t) \tag{7}.$$

The frequencies and the modes of natural vibration are analyzed by using Holzer-Myklestadt method.[10] By using these natural frequencies and modes, the ordinary differential equations of the second order are derived from the equations of motion (A-1 ~ A-3). For the seesaw blade, there are two kinds of modal series as follows[11]:

$$\{w_c(r,t), v_c(r,t), \phi_c(r,t)\}^T = \sum_{j=1}^{j_R} \{\hat{w}_j^R(r), \hat{v}_j^R(r), \hat{\phi}_j^R(r)\}^T q_j^R(t)$$

$$+ \sum_{j=1}^{j_A} \{\hat{w}_j^A(r), \hat{v}_j^A(r), \hat{\phi}_j^A(r)\}^T q_j^A(t) \tag{8}$$

where $(\ )^R$ and $(\ )^A$ show "the rigid modal series" and "the articulated modal series", respectively. The rigid modal series satisfies the boundary conditions at the blade root, displacement =moment=0, for all three degrees of freedom. The articulated modal series satisfies the boundary conditions at the blade root, displacement = slope = 0 for flapping, and displacement = moment = 0 for lagging and torsion. These two modal series are shown in Fig. 3(a) and 3(b). As shown in Appendix B, two sets of the

differential equations are derived for the two modal series, respectively. These equations are numerically calculated by coupling with aerodynamic and inertial forces and moments given by the LCM.

4. Flutter Boundary for a Hingeless Blade

By using the present method, the analytical study has been conducted for a real rotor defined in Table 1 in order to make clear the effect of the blade elasticity on the design of wind turbine. The sensitivity of related parameters for the flutter boundary is investigated by changing the values of the following parameters: such as rigidity, pitch angle, position of the center of gravity and position of the elastic axis of the blade. The inflow ratio is changed in this calculation in the manner that the wind velocity is varied while the rotational speed is kept constant at the design maximum speed, $\Omega = 9.42$ rad/s. Three components of the rigidity of the real rotor, $(EI_y)_0$, $(EI_z)_0$ and $(GJ)_0$ were determined by the critical load of the steady aerodynamic moment at the blade root multiplied by a certain factor of safety. As shown in Fig. 4, the flutter does not occur for this original rigidity. The three components of the rigidity, flapwise bending, lead-lag bending and torsion are, then, reduced simultaneously until the flutter occurs. In addition, the position of the chordwise center of gravity and the position of the elastic axis are changed from the original locations, both of which are 40% chord from the leading edge. It is indicated in Fig. 4 that the position of the center of gravity relative to the elastic axis is the most sensitive parameter to the flutter. In addition, the larger pitch angle, the lower wind velocity and the larger rigidity make the blade more stable for the flutter. If the consideration is concentrated to the safety of the blade flutter, and if the positions of the center of gravity and the elastic axis locate ahead of 40% chord, the three components of the rigidity of the original rotor may reduce to one tenth. The other factors, however, sometimes restrict this reduction of the rigidity as follows.

An effect of change of rigidity on the flapwise and torsional displacements at the blade tip is shown in Fig. 5. As the rigidity is reduced, all displacements, specifically the torsional angle, increase for this exemplified blade, the center of gravity of which is located at the 40% chord position. This causes the difficulty of the pitch control of the blade, and it is impossible to realize the reduction of the rigidity until the point at which the flutter occurs. This limit caused by torsional displacement is drastically improved by shifting the center of gravity and the elastic axis to 30% chord position, as shown in Fig. 5. However, the flapwise displacement at the blade tip is not improved by this modification. Comparing this displacement with the distance between the blade tip and the tower of the wind turbine, it is concluded that the flapwise displacement does not cause any serious problem in this blade.

Another factor to be considered is the three components of maximum stress caused by the flapwise bending, chordwise bending and torsional moments. The maximum stress is usually checked at the following two operating conditions: The one is the non-rotating state where the maximum wind velocity ever observed should be adopted. At this state, the three components of maximum stress are just inversely proportional to the rigidity. The other operating condition is the rotating state where the maximum wind velocity may be determined by the designer as the design maximum wind velocity. The operation stops when the wind velocity becomes larger than this design maximum wind velocity. At this rotating state, the maximum stress of the flapwise bending, which is usually the most severe component among the three, changes complicatedly as the rigidity becomes weak. This stress is proportional to the flapwise bending moment and is inversely proportional to the rigidity. The flapwise bending moment is composed of the aerodynamic bending moment and the moment caused by the centrifugal force. Fig. 6 shows the variations of these components of the bending moment at the blade root. It is observed that the aerodynamic moment is relaxed by the moment of the centrifugal force as the rigidity becomes weak. Therefore, the maximum stress of the bending moment is roughly five times as large as the original value, when the rigidity becomes one tenth as shown in Fig. 6.

In addition to the factors stated above, the fatigue failure caused by the unsteady airloading, which is generated by the gust or the yawed wind, should be considered. The analytical method and the step response for this unsteady air-loading were already presented.[12] The procedure taking the blade elasticity into design consideration is, then, summarized as shown in Fig. 7. The re-design of the exemplified real rotor was attempted by following this flow chart. The result indicates that the rigidity and the mass of the blade may be reduced to half values of the original blade. In addition, it is recommended that the chordwise center of gravity and the elastic axis should locate near the elastic axis and the aerodynamic center, respectively.

5. Flutter Boundary for a Seesaw Blade

In order to make clear the difference between the seesaw and hingeless blades, the analytical study for the flutter boundary has been conducted for the seesaw blade. An exemplified blade given in Table 1 is modified for the seesaw blade only by changing the root constrained condition. Results are shown in Fig. 8. It is observed that as far as concerning the flutter boundary the rigidities must be kept in higher values for the seesaw blade than those for the hingeless blade.

6. Conclusions

By using the LCM, an analytical study has been conducted in order to specify the flutter boundary. In comparison with the previous other works in this research field, the LCM has

capability of taking the precise induced velocity distribution into calculation. It is obtained that the position of center of gravity relative to the elastic axis is the most sensitive parameter to the flutter. The difference of the flutter boundary between hingeless and seesaw blades are also remarkable. The seesaw blade shows the more unstable characteristics for the flutter. This indicates that the rigidities must be kept in higher values for the seesaw blade than those for hingeless blade as far as concerning the flutter boundary. The larger pitch angle, the lower wind velocity and the larger rigidity make the blade more stable for the flutter. The position of the elastic axis relative to the aerodynamic center has the strong effect on the pitch divergence or the torsional displacement which sometimes makes the pitch control difficult. The flap-wise bending moment strongly depends on the flapwise displacement, because this displacement generates the flapwise bending moment caused by the centrifugal force.

Taking these aeroelastic parameters into blade design, the flow chart of the design procedure was presented. The redesign of the exemplfieid blade was attempted by following this procedure. The result indicates that the rigidity and the mass of the blade may be reduced to half values of the original blade. In addition, it is recommended that the chordwise center of gravity and the elastic axis should locate near the elastic axis and the aerodynamic center respectively.

Appendix A.   Equations of Blade Elasticity

According to the x-y-z coordinate system shown in Fig. A-1, the equations of the blade elasticity are given by

$$[EI_{yz}v''_c + EI_y w''_c]'' - (Tw'_c)' + m(\ddot{w}_c + \bar{e}_y \ddot{\phi}_c)$$
$$+ [\bar{I}_y(-\ddot{w}'_c + \Omega^2 w'_c) + \bar{I}_{yz}(-\ddot{v}'_c + \Omega^2 v'_c) - m\bar{e}_y r\Omega^2 \phi_c - m\bar{e}_z(-\ddot{u}_c + \Omega^2 u_c)]'$$
$$= F_z \tag{A-1}$$

$$[EI_z v''_c + EI_{yz} w''_c]'' - (Tv'_c)' + m[\ddot{v}_c - \Omega^2 v_c - \bar{e}_z(\ddot{\phi}_c - \Omega^2 \phi_c)]$$
$$- [\bar{I}_z(\ddot{v}'_c - 2\Omega^2 v'_c) + \bar{I}_{yz}(\ddot{w}'_c - 2\Omega^2 w'_c) - m\bar{e}_y(\ddot{u}_c - \Omega^2 u_c) - m\bar{e}_z r\Omega^2 \phi_c]'$$
$$= F_y \tag{A-2}$$

$$- [(GJ + Tk_A^2)\phi'_c]' + Te_{Az}v''_c - Te_{Ay}w''_c + \bar{I}_x \ddot{\phi}_c + (\bar{I}_z - \bar{I}_y)\Omega^2 \phi_c$$
$$+ m[\bar{e}_y(\ddot{w}_c + r\Omega^2 w'_c) + \bar{e}_z(-\ddot{v}_c + \Omega^2 v_c - r\Omega^2 v'_c)]$$
$$= N_x \tag{A-3}$$

where the external forces and moment are given by

$$F_z = L_z - mr\Omega^2\beta_p + [m\bar{e}_z r\Omega^2 + 2\bar{I}_y\Omega\dot{\phi}_c - 2m\bar{e}_z\Omega\dot{v}_c]' + mg\beta_p\sin\psi \tag{A-4}$$

$$F_y = L_y - m\bar{e}_y\Omega^2 + [m\bar{e}_y r\Omega^2 + 2\bar{I}_{yz}\Omega\dot{\phi}_c - 2m\bar{e}_y\Omega\dot{v}_c]' + mg\cos\psi \tag{A-5}$$

$$\left. \begin{aligned} N_x &= M_x - \bar{I}_{yz}\Omega^2 + m\bar{e}_z\bar{e}_y\Omega^2 + 2\Omega(\bar{I}_y\dot{w}_c' + \bar{I}_{yz}\dot{v}_c') - 2m\bar{e}_z\Omega\dot{u}_c \\ &\quad - m\bar{e}_y r\Omega^2\beta_p \end{aligned} \right\} \tag{A-6}$$

Appendix B. The Ordinary Differential Equations for Seesaw Blade

Following the procedure of calculation given by ref. 11, the relation is obtained for "rigid modal series" and "articulated modal series" as follows:

$$\left. \begin{aligned} q_j^R(\psi) &= q_j^R(\psi + \pi) \\ q_j^A(\psi) &= -q_j^A(\psi + \pi). \end{aligned} \right\} \tag{B-1}$$

By substituting equation (8) into equation (A-1) ~ (A-3), and by using equation (B-1) and orthogonal conditions between the natural modes, the ordinary differential equation are derived as,

$$\left. \begin{aligned} M_j^R(\ddot{q}_j^R + \omega_j^{2R} q_j^R) &= Q_j^R \\ \\ M_j^A(\ddot{q}_j^A + \omega_j^{2A} q_j^A) &= Q_j^A \end{aligned} \right\} \tag{B-2}$$

where

$$\begin{aligned} M_j^R &= \int_o^R (\bar{I}_x\hat{\phi}_j^R + m\bar{e}_y\hat{w}_j^R\hat{\phi}_j^R - m\bar{e}_z\hat{v}_j^R\hat{\phi}_j^R)\,dr \\ &\quad + [\int_o^R\{m(\hat{w}_j^{2R} + \bar{e}_y\hat{\phi}_j^R\hat{w}_j^R) + (\bar{I}_y\hat{w}_j'^R + \bar{I}_{yz}\hat{v}_j'^R)\hat{w}_j'^R\}\,dr \\ &\quad - \{(\bar{I}_y\hat{w}_j'^R + \bar{I}_{yz}\hat{v}_j'^R)\hat{w}_j^R\}_o^R] \\ &\quad + \int_o^R\{m(\hat{v}_j^{2R} - \bar{e}_y\hat{\phi}_j^R\hat{v}_j^R) + (\bar{I}_z\hat{v}_j'^R + \bar{I}_{yz}\hat{w}_j'^R)\hat{v}_j'^R\}\,dr \\ &\quad - \{(\bar{I}_z\hat{v}_j'^R + \bar{I}_{yz}\hat{w}_j'^R)\hat{v}_j^R\}_o^R] \end{aligned} \tag{B-3}$$

$$Q_j^R = \frac{1}{2} \left[\int_o^R \{N_x (\psi) + N_x (\psi + \pi)\} \hat{\phi}_j^R \, dr \right.$$

$$+ \int_o^R \{F_z(\psi) + F_z (\psi + \pi)\} \hat{w}_j^R \, dr$$

$$\left. + \int_o^R \{F_y(\psi) + F_y (\psi + \pi)\} \hat{v}_j^R \, dr \right] \qquad \text{(B-4)}$$

$$M_j^A = \int_o^R (\bar{I}_x \hat{\phi}_j^{2A} + m\bar{e}_y \hat{w}_j^A \hat{\phi}_j^A - m\bar{e}_z \hat{v}_j^A \hat{\phi}_j^A) \, dr$$

$$+ \left[\int_o^R \{m(\hat{w}_j^{2A} + \bar{e}_y \hat{\phi}_j^A \hat{w}_j^A) + (\bar{I}_y \hat{w}_j'^A + \bar{I}_{yz} \hat{v}_j'^A) \hat{w}_j'^A\} \, dr \right.$$

$$\left. - \{(\bar{I}_y \hat{w}_j'^A + \bar{I}_{yz} \hat{v}_j'^A) \hat{w}_j^A\}_o^R \right]$$

$$+ \int_o^R \{m(\hat{v}_j^{2A} - \bar{e}_z \hat{\phi}_j^A \hat{v}_j^A) + (\bar{I}_z \hat{v}_j'^A + \bar{I}_{yz} \hat{w}_j^A) \hat{v}_j'^A\} \, dr$$

$$- \{(\bar{I}_z \hat{v}_j'^A + \bar{I}_{yz} \hat{w}_j'^A) \hat{v}_j^A\}_o^R \right] \qquad \text{(B-5)}$$

$$Q_j^A = \frac{1}{2} \left[\int_o^R \{N_x (\psi) - N_x (\psi + \pi)\} \hat{\phi}_j^A \, dr \right.$$

$$+ \int_o^R \{F_z (\psi) - F_z (\psi + \pi)\} \hat{w}_j^A \, dr$$

$$\left. + \int_o^R \{F_y (\psi) - F_y (\psi + \pi)\} \hat{v}_j^A \, dr \right] \qquad \text{(B-6)}$$

REFERENCES

1. A. M. Feingold, Theory of Mechanical Oscillations of Rotors with Two Hinged Blades, NACA Wartime Report ARR No. 3I13 (1943).

2. D. A. Peters and K. Hohenemser, Application of the Floquet Transition Matrix to Problems of Lifting Rotor Stability, J. of the AHS, Vol. 16, No. 2 (1971), pp. 25-33.

3. P. Friedmann and C. E. Hammond, Efficient Numerical Treatment of Periodic Systems with Application to Stability Problems, International J. for Numerical Methods in Engineering, Vol. 11 (1977), pp. 1117-1136.

4. C. J. Astill and C. F. Niebanch, Prediction of Rotor Instability at High Forward Speeds, Vol. II, Classical Flutter, USAAVLABS, TR 68-18B, AD 683861 (1969).

5. K. W. Shipman and E. R. Wood, A Two-Dimensional Theory for Rotor Blade Flutter in Forward Flight, J. of Aircraft, Vol. 8, No. 12 (1971), pp. 1008-1015.

6. K. Kawachi, A. Azuma and I. Watanabe, Study of Bending-Torsion Flutter of a Wind Turbine, 12th European Rotorcraft Forum, F. R. Germany (1986).

7. A. Azuma, K. Kawachi and A. Ito, Application of the Local Circulation Method to the Flutter Analysis of Rotary Wings, 8th European Rotorcraft Forum, Paper No. 3.12 (1982).

8. K. Kato, A Numerical Approach to the Unsteady Aerodynamic Forces of the Helicopter Rotor Blade. J. of Japan Society for Aeronautical and Space Sciences, Vol. 22, No. 247, (1974), pp. 390-397, in Japanese.

9. R. L. Bisplinghoff, et al., Aeroelasticity, Addison-Wesley (1955).

10. N. O. Myklestad, Fundamentals of Vibration Analyses, McGraw-Hill (1944).

11. N. Kawakami, Dynamics of an Elastic Seesaw Rotor, J. of Aircraft, Vol. 14, No. 3 (1977), pp. 291-300.

12. A. Azuma and S. Saito, Dynamic Response of Windturbine to Yawed Wind, 10th European Rotorcraft Forum, The Netherlands (1984).

Table 1   Dimensions of an exemplified blade.

Items	Dimensions
Rotor radius	7m
Blade mass	122kg
No. of blades	2
Preconing angle	0.0deg.
Wing section	NACA 4418
Mean chord	0.528m
Angle of twist	29.5deg.
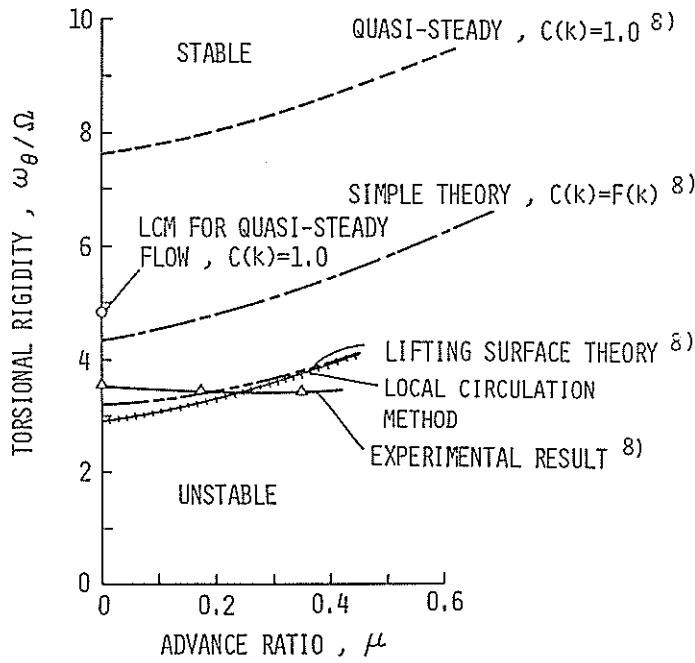
Figure 1   Flutter boundary of a helicopter rotor.[7]
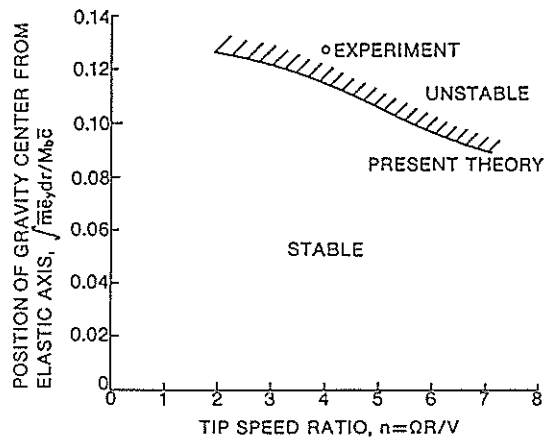
Figure 2   Flutter boundary of a wind turbine.[6]
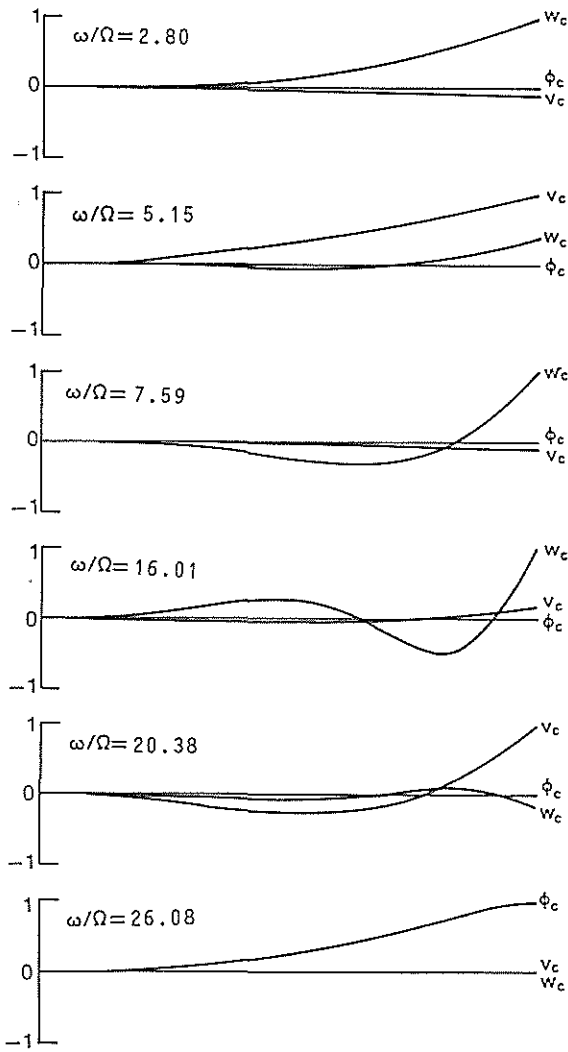
Figure 3(a)   Natural frequency and mode
               (Rigid modal series)
               $\Omega = 9.42$ rad./s.
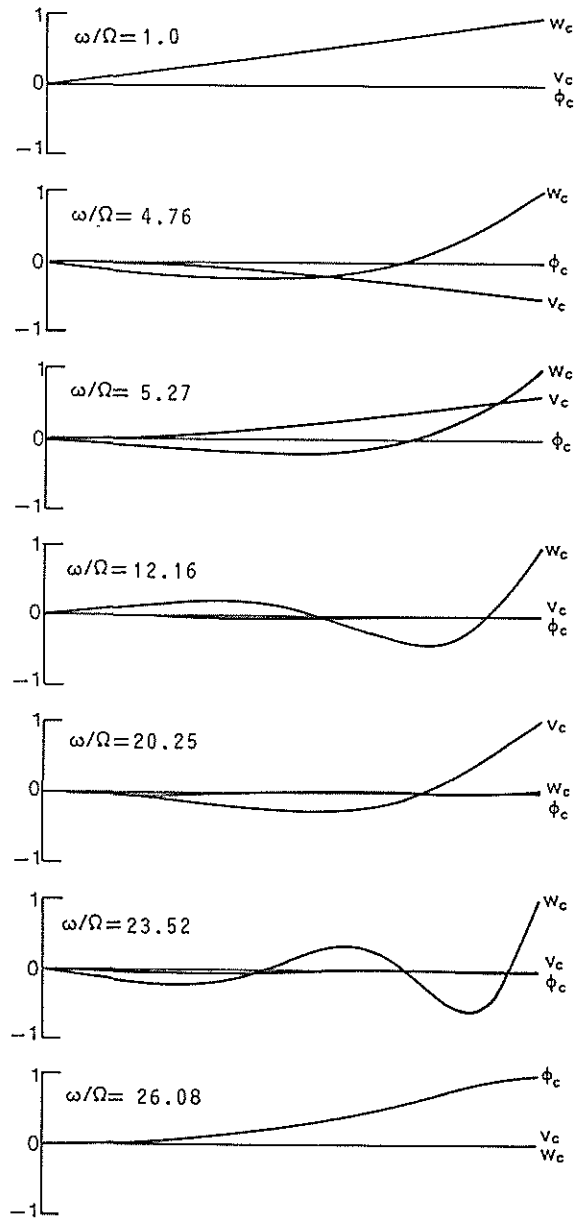
Figure 3(b)   Natural frequency and mode
               (Articulated modal series)
               $\Omega = 9.42$ rad./s.
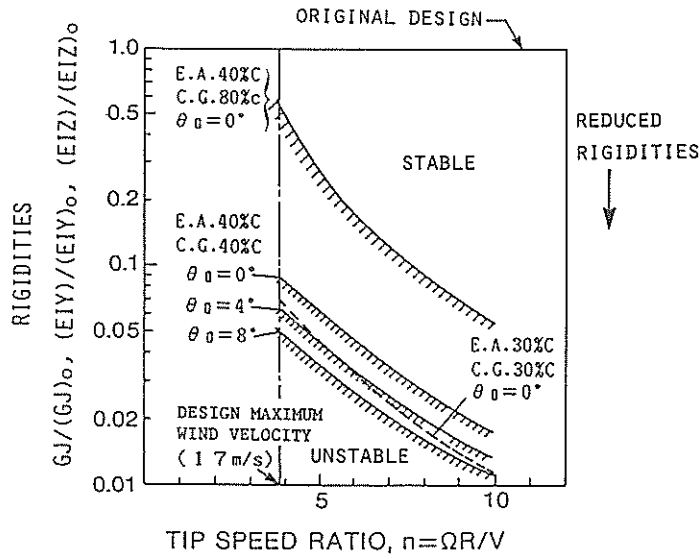
Figure 4   Flutter boundary for a hingeless blade.
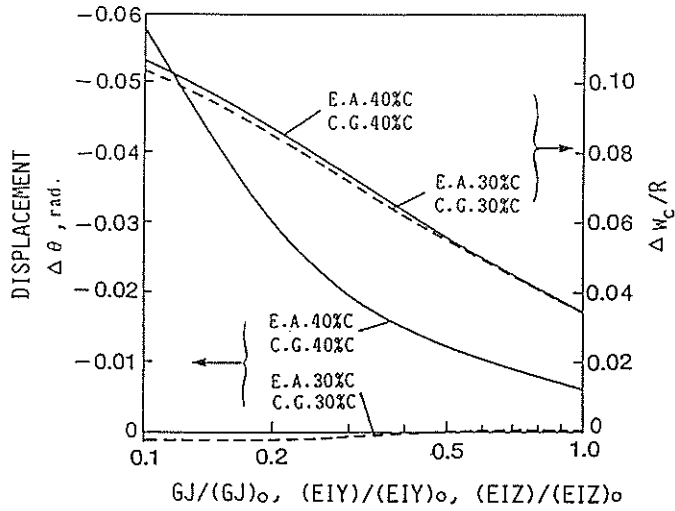
Figure 5   Displacement at blade tip.
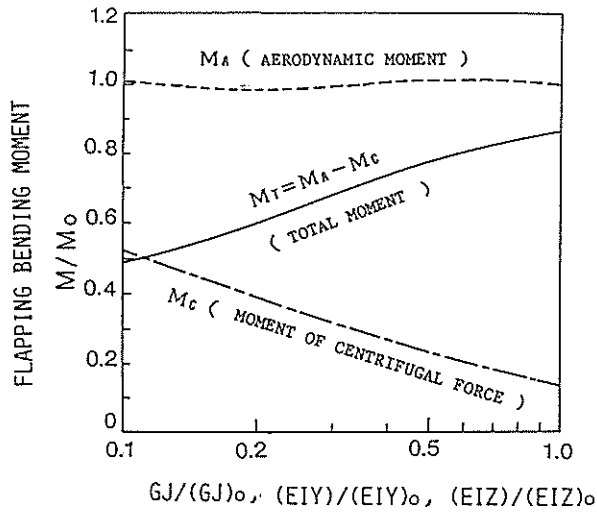
Figure 6   Bending moment at blade root.
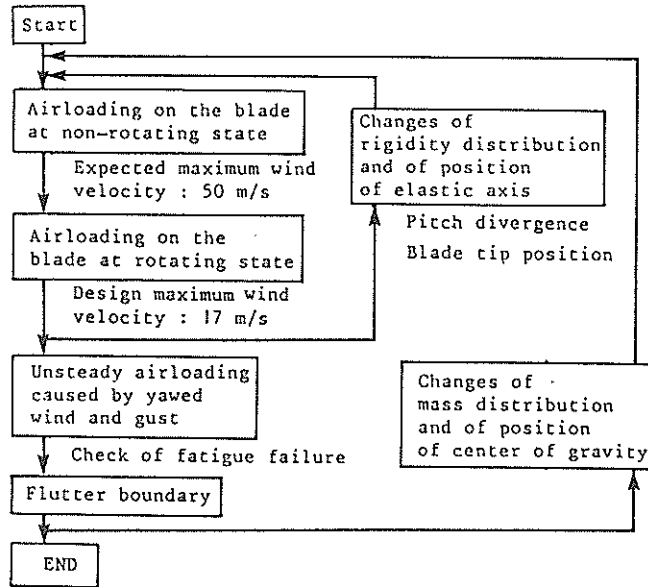
Figure 7　Design Procedure.
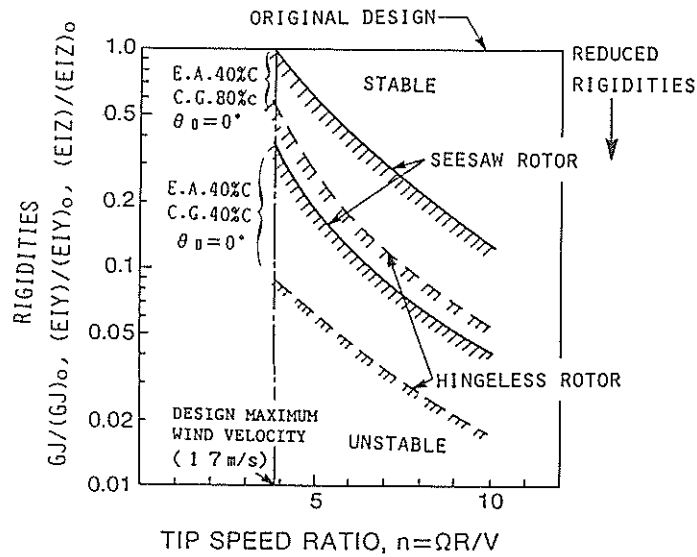
Figure 8　Flutter boundary for a seesaw blade.
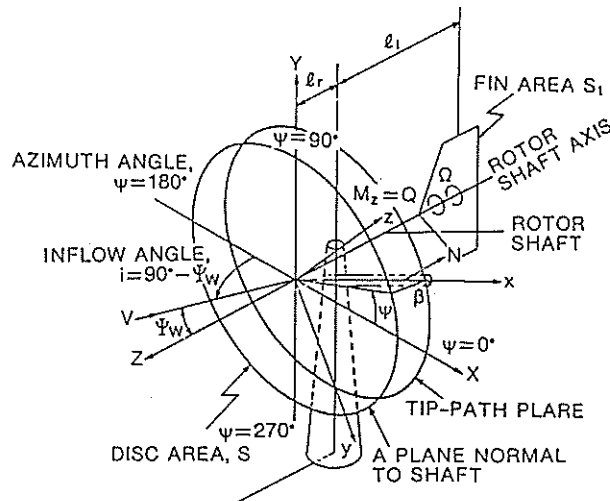
Figure A.1.　Wind turbine and coordinate system.